Li-ion Battery Cooling - A Computational Study of Different Phase Change Material Configurations

Sumudu Adikaram[a], Adel Nasser[b], Cristina Vallés[c], Chamil Abeykoon[a*]

[a] Northwest Composites Centre, Henry Royce Institute and National Graphene Institute, Department of Materials, Faculty of Science and Engineering, The University of Manchester, Oxford Road, Manchester, M13 9PL, UK
[b] Department of Mechanical and Aerospace Engineering, Faculty of Science and Engineering, The University of Manchester, Oxford Road, Manchester, M13 9PL, UK
[c] Department of Materials, National Graphene Institute and Henry Royce Institute, University of Manchester, Oxford Road, Manchester, M13 9PL, UK
sumudu.adikaram@manchester.ac.uk, a.g.nasser@manchester.ac.uk, cristina.valles@manchester.ac.uk, chamil.abeykoon@manchester.ac.uk*

ABSTRACT

Overheating of Li-ion batteries in Electric Vehicles (EVs) degrades performance and reduces lifespan. Hence, energy-efficient and reliable Battery Thermal Management Systems (BTMS) are required. This paper investigates the use of Phase Change Materials (PCMs), a passive cooling method with high heat storage capacity, for the thermal management of prismatic Li-ion battery cells in EVs. This computational study models the influence of buoyancy-driven convective flow on the PCM cooling performance, compared against thermal conduction-only models. In addition, this study investigates how convective flow influences the cooling performance with variations in cell orientation between vertical and horizontal alignments. n-Octadecane is used as the PCM, and Computational Fluid Dynamics (CFD) simulations were conducted with the Solidification and Melting model in ANSYS Fluent. A 12 mm PCM layer placed around the cell periphery reduced the centre temperature after 1800 s by 2.7 K in the vertical orientation and 3.7 K in the horizontal orientation compared to air-cooling. The effect of natural convection was more pronounced in the horizontal orientation, providing superior cooling performance relative to the vertical case. When the same PCM volume was used to fully enclose the cell, the cooling effect was further enhanced, achieving a maximum temperature reduction of 8.3 K within the first 1800 s. The findings demonstrate that natural convection significantly enhances the PCM-based cooling effectiveness, particularly in horizontally oriented cells, while thinner PCM layers with increased heat transfer area promote faster melting and improved cooling performance.

KEYWORDS: *Battery Thermal Management (BTMS), Phase Change Materials (PCMs), Natural Convection, Computational Fluid Dynamics (CFD), Prismatic Li-ion Cells*

INTRODUCTION

Li-ion batteries are popular in EVs due to their high energy densities and long operating life (Subramanian et al., 2021). However, these batteries tend to overheat during charging and operation, while the overheating of one cell can lead to thermal runaway of the whole battery pack (Shirazi et al., 2016). Hence, it is important to maintain the temperature of the battery cells within the recommended range, usually below 40 °C for effective operation (Subramanian et al., 2021). Furthermore, monitoring the battery cells and regulating their temperature within the optimal limits helps to extend their life (Warner, 2014). Another key design criterion for BTMS is to control the temperature change of the battery pack within a 2-5 °C difference throughout its lifetime (Warner, 2014). The cooling requirement also depends on the region of operation and the nature of its performance (Warner, 2014), as the heating rates of the battery vary due to both the ambient

https://doi.org/10.54389/MYTF4946

temperature and the charging and discharging rates.

With increased energy efficiency and fuel economy becoming rising priorities in the world, passive cooling methods are becoming an ideal solution for thermal management of EV batteries as they do not consume extra energy (Jankowski & McCluskey, 2014). Furthermore, they can offer cost-effective and easy installation solutions without complicating the design (Li et al., 2025). However, passive air cooling does not provide sufficient cooling for EV batteries; hence, alternative cooling methods are required.

Phase Change Materials (PCMs) are popular for thermal management and heat storage due to their high heat storage densities, as they absorb and release heat as latent heat while going through a phase change. They become good passive cooling options due to their high heat-absorbing and constant temperature heat storage capabilities, and hence, are currently under a lot of research. They are ideal for EV battery cooling as they are less bulky, less complex and less expensive than forced air cooling systems and liquid cooling methods (Jaguemont et al., 2018).

This work involves modelling a PCM cooling unit for prismatic Li-ion battery cells, which are widely used in EVs due to their high-density energy storage capabilities. The study is conducted to evaluate the cooling performance of different PCM unit designs with varying PCM layer thicknesses and configurations. The effect of gravity on the cooling performance of the PCM unit was also evaluated for different orientations of the battery cell. Two studies that have been conducted on the same battery model by Javani et al. (2014) and Verma et al. (2019) were used as the basis to develop the numerical model, which is detailed below.

Javani et al. (2014) studied the thermal performance of the battery with PCM unit under different heat generation rates of the cell caused by different operational conditions and ambient temperatures. The authors evaluated the cooling performance variation under different PCM thicknesses of 3, 6, 9 and 12 mm. Here, n-Octadecane was used as the PCM, and the PCM layer was only added around the periphery of the battery (refer to Figure 27) due to the orthotropic nature of the thermal conductivity of the prismatic-type battery cell (Javani et al., 2014; Li et al., 2025). Furthermore, the authors only modelled the thermal conduction, ignoring the effects of the convective flow of the liquid PCM. The temperature variation of the battery at fixed points was observed in the study to analyse the PCM cooling performance. The authors found that the maximum temperature reduction of the battery after 20 minutes only improved from 2.77 K to 3.04 K when the PCM thickness was increased from 3 mm to 12 mm. Furthermore, Javani et al. (2014) defined constant values for the specific heat (C_P), thermal conductivity and the density of the PCM for each region, solid, liquid and phase transition, as step functions. This approach is not suitable for modelling the PCM with gravity effects for tracking the flow front and to model the buoyancy-driven flow (Pan et al., 2018).

Verma et al. (2019) used the same battery model and extended the study using a different PCM, Capric acid. They observed the PCM cooling performance with the thickness of the PCM layer varying from 3, 7, 9 and 12 mm. Furthermore, the cooling performance was studied under two ambient conditions: 294 K for normal conditions and 323 K for desert conditions. It was

concluded that the PCM layer with a 3 mm thickness provides the optimum cooling. Similar to the previous study, Verma et al. (2019) have not considered the PCM flow in the model. Contrastingly, Verma et al. (2019) used constant values for the PCM properties of C_P, density and the thermal conductivity and used the Solidification and Melting model in ANSYS Fluent. However, despite the difference in the model, it was validated using the results of Javani et al. (2014), with an error below 7%.

In this study, the same battery model was used with n-Octadecane as the PCM. The model was improved to analyse the convection effects of the liquid PCM on its melting rates and the cooling performance. Effects of gravity and temperature-dependent density variations were incorporated into the model to simulate the buoyancy-driven convective flow and its effects. Furthermore, the orientation of the battery affects the PCM performance when convective flow is present. Due to the stacking of battery cells when creating the battery pack, vertical orientation is preferred for prismatic-type cells, where horizontal cell orientation is avoided to prevent upper cells from exerting force on the lower cells. Hence, vertical cell orientation is also modelled in comparison with the horizontal orientation. Finally, the study evaluates the effect of PCM configuration, i.e. PCM around the periphery of the cell (**Side Pack**) and PCM around the entire cell (**Whole Pack**), to understand how increasing the heat transfer surface area while reducing the PCM layer in the direction of high thermal conductivity influences the cooling performance.

METHODOLOGY

Initially, the model was created similarly to the models by Javani et al. (2014) and Verma et al. (2019), neglecting the convective flow for validating the initial model. Later, the gravity effects and density variation were incorporated into the model to analyse the convective flow effects.

Design

The parameters of the battery and the performance conditions were taken from Javani et al. (2014). The cell dimensions used in the models are provided in Table 24. The models and their boundary conditions are presented in

Figure 27. Five PCM configurations were analysed, and their thermal performance was compared, namely, the air-cooled battery without PCM cooling (**Cellw/oPCM**), the battery with PCM cooling without convective flow analysis (**noFlow**), and the battery with PCM cooling with convective flow analysis in the vertical orientation (**FlowY**) and the horizontal orientation (**FlowZ**). Finally, the same PCM volume was applied around the entire cell (except for the terminal face) to create the **WholePack** configuration, which includes a thin layer of PCM around the cell as shown in

Figure 27 (b). The performance of the WholePack configuration was compared to the **SidePack** configurations, i.e. noFlow, Flow Y and FlowZ, where the PCM only lies around the periphery of the cell as shown in

Figure 27 (a). Here, the thickness of the WholePack configuration was set so that the total PCM volume matched that of the SidePack configuration.

Table 24. Battery cell dimensions

Component	**Length (mm)**	**Height (mm)**	**Thickness (mm)**
Cell	146	194	5.4
Terminals	35	15	0.6
PCM (SidePack config)	3 and 12 mm around the periphery of the cell		5.4
PCM (WholePack config)	0.6 mm around the entire cell (except the face with terminals)		

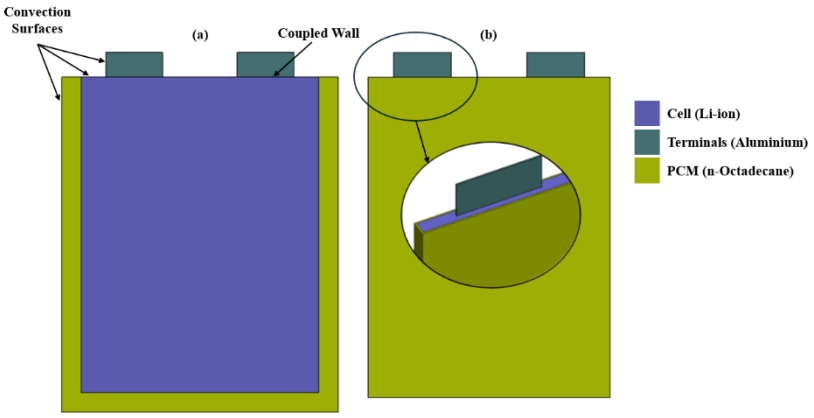

Figure 27. Geometry and boundary conditions of a) SidePack, b) WholePack configurations

Table 25. Boundary conditions

Initial cell temperature & ambient temperature	294.15 K

Uniform heat generation in the cell (when the battery is discharging at a 2C rate)	63,970 W/m^3
Outer surfaces (PCM walls, terminals & the cell top)	Convection
	Heat transfer coefficient: 7 W/m^{2}K
Coupled wall between the cell and the terminal	
Terminals: no heat generation, acts as cooling fins, material- Aluminium	
The PCM compartment and the cell are covered by a thin Aluminium layer of 0.5 mm thickness, which acts as the convection surface.	

The boundary conditions used for the simulations are provided in Table 25. The specifications of the battery, taken from Javani et al. (2014), are shown in Table 26. The heat generation rate when the battery is discharging at a 2C rate is 63,970 kW/m^3, which is 4.45 W per cell. The 2C rate signifies the battery discharges completely within half an hour. This rate was used for the simulations first to validate the results with the two previous studies, and then to compare the results of different cooling configurations with the initial results. Furthermore, at this high discharge rate, the battery tends to heat up more than the desired levels; hence, cooling is important.

Table 26. Battery Specifications

Heat generation rate (considered to be uniform throughout the cell)	At standard working conditions	6855 W/m^3
	When the cell is discharged at a 2C rate	63,970 W/m^3
	At full power	200,000 W/m^3
Thermal conductivity of the cell (Orthotropic)	In planar directions	25 W/m K
	In the direction normal to the cell	1 W/m K
Specific heat capacity (C_P)		1097 J/kg K
Density		1881 kg/ m^3

n-Octadecane was used as the PCM, and its properties are shown in Table 27. The Boussinesq model is used to approximate the density variation with temperature. Data was not available for the viscosity and thermal expansion coefficient of n-Octadecane in the paper by Javani et al. (2014); hence, it was taken from G. Zaki, E., & S. Dhmees (2022).

Table 27. Properties of n-Octadecane (Javani et al., 2014)

Solidus temperature ($T_{solidus}$)	301.15 K
Liquidus temperature ($T_{liquidus}$)	303.15 K
Thermal conductivity (k)	0.152 W/m K
Latent heat (L)	225 kJ/kg
Specific heat capacity (C_P)	2180 J/kg K
Density (ρ)	724 kg/ m^3
Viscosity	3.878×10^{-3} Pa s (G. Zaki, E., & S. Dhmees, 2022)
Thermal expansion coefficient	0.00091 1/K (G. Zaki, E., & S. Dhmees, 2022)

Mathematical Model

Initially, the noFlow configuration was modelled, neglecting the PCM convective flow, similar to the assumptions made in the previous two studies, to validate the results using those of the two papers. The density was considered constant, and only the thermal conduction was modelled. This method is called the Effective Heat Capacity (EHC) method. Here, only the energy equation is solved, where the phase change process is incorporated in the model with varying thermophysical properties defined. This model requires less computational power and permits larger mesh and time step sizes.

However, when modelling the Solidification and Melting of PCM with the convective flow, the Enthalpy Porosity (EP) method was used. The phase change behaviour was modelled using the Solidification and Melting model in ANSYS Fluent. The liquid front was modelled as an enthalpy-porosity formulation. The solid-liquid mushy zone is modelled as a porous zone with its porosity equal to the liquid fraction (a value between 0 and 1) of each cell in the domain. PCM is considered to be Newtonian and incompressible. The density variations are only considered in the buoyancy source term and are modelled using the Boussinesq model. Transient simulations were used to model the melting of the PCM over time with a **laminar viscous model.**

Enthalpy of the material (H) is calculated as the sum of sensible enthalpy (h) and the latent heat enthalpy (ΔH) and is given in Eq. (1). h is calculated by Eq. (2).

$$H = h + \Delta H \quad (1)$$

$$h = h_{ref} + \int_{T_{ref}}^{T} C_P dT \quad (2)$$

Here, h_{ref} is the reference enthalpy, T_{ref} is the reference temperature and C_P is the specific heat at constant pressure. The liquid fraction β is calculated using the PCM temperature (T) as given in the set of equations in Eq. (3).

$$\beta = 0 \text{ if } T < T_{solidus} \quad (3)$$

$$\beta = 1 \text{ if } T > T_{liquidus}$$

$$\beta = \frac{T - T_{solidus}}{T_{liquidus} - T_{solidus}} \text{ if } T_{solidus} < T < T_{liquidus}$$

The latent heat enthalpy (ΔH) can be calculated as given by Eq. (4).

$$\Delta H = \beta L \quad (4)$$

Here, L is the latent heat of the PCM, and the latent heat enthalpy changes from 0 to L as the solid PCM melts to become a liquid. The continuity equation, which ensures mass conservation, is given by Eq. (5), where the mass flux divergence is made zero. Here, density (ρ) is considered a constant, which is the reference density.

$$\nabla \cdot \rho \vec{v} = 0 \quad (5)$$

The momentum equation, which models the motion of PCM including inertia, viscous forces, and buoyancy forces due to thermal expansion, is given by Eq. (6). Here, the Boussinesq approximation is used to calculate the buoyancy force, where γ is the thermal expansion coefficient. $\vec{S}$ is the sink term, which is defined in Eq. (7).

$$\rho \frac{\partial \vec{v}}{\partial t} + \rho(\vec{v} \cdot \nabla)\vec{v} = -\nabla P + \mu(\nabla^2 \vec{v}) - \rho\gamma\left(T - T_{ref}\right)\vec{g} - \vec{S} \quad (6)$$

$$S = \frac{(1-\beta)^2}{(\beta^2 + \epsilon)} A_{mush} \cdot \vec{v} \quad (7)$$

The sink term calculates the momentum sink due to the reduced porosity in the mushy zone. Here, ε is a small number (0.001) to prevent division by zero, $\vec{v}$ is the velocity due to the buoyancy-driven natural convection and A_{mush} is the mushy zone constant. The mushy zone constant was selected as 100000. This parameter determines how quickly the velocity drops to zero as the material solidifies. For PCMs, the value is typically set to 100000 (Li et al., 2025).

The energy equation, which considers conduction and convection, is given by Eq. (8).

$$\frac{\partial}{\partial t}(\rho H) + \nabla \cdot (\rho \vec{v} H) = \nabla \cdot (k \nabla T) - S_L \quad (8)$$

Here, H is the enthalpy (from Eq. (1)), ρ is the density, $\vec{v}$ is the local velocity vector (initially in no flow condition, this was assumed to be 0), k is the thermal conductivity and S_L is the source term that accounts for the latent heat release and absorption during phase transition, which is given by Eq. (9). Here, ε is the porosity, which is equal to the liquid fraction.

$$S_L = \frac{\varepsilon \partial \rho \beta L}{\partial t} + \nabla(\rho \vec{v} \beta L) \quad (9)$$

It is important to capture convective flow as it promotes mixing, which could either even out the temperature gradients or could adversely affect the even cooling of the cell. Therefore, excluding the PCM flow can lead to inaccurate results.

Computational Setup

A structured mesh was used as presented in **Error! Reference source not found.**.

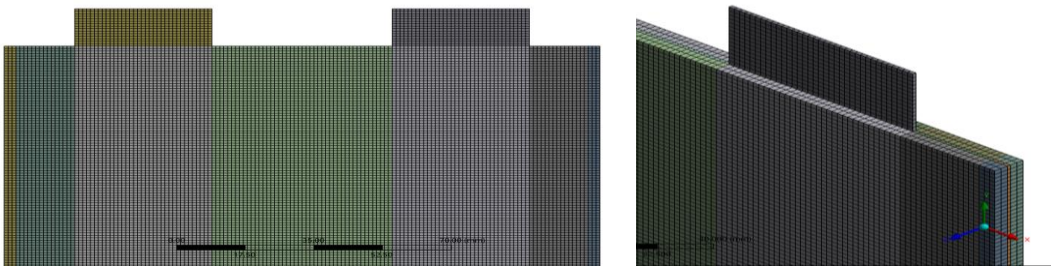

Figure 28. Structured mesh used for the cell-PCM model

All results were generated for five points along the centreline of the cell, as shown in Figure 29, which shows the plane midway across the thickness of the battery. The distances to Points 1-5 are 184, 140.5, 97, 43.5, and 10 mm, respectively, from the bottom edge of the cell.

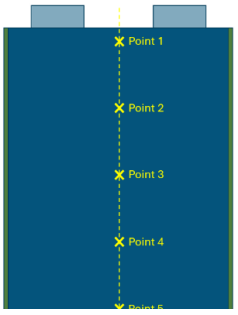

Figure 29. Locations along centreline to monitor data

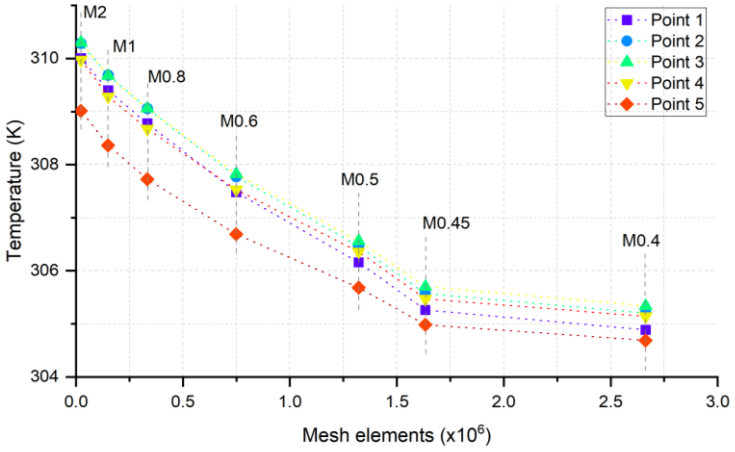

A grid independence study was performed for the EP model, which is presented in **Error! Reference source not found.**, and t he mesh size of 0.6 mm was selected for the simulations. This size provided reliable results with an error of less than 0.85% while minimising computational cost. Since the study focuses on a qualitative comparison between different configurations, the same mesh element size was applied consistently across all simulations.

Validation

First, the model without PCM convection was validated using the results of the two papers, Javani et al. (2014) & Verma et al. (2019). The validation process was carried out initially for the air-cooled cell without PCM cooling (**Error! Reference s ource not found.**(a)), followed by the cell with PCM cooling with a 3 mm thick PCM layer (**Error! Reference source not found.**(b)). Since the EHC model has a reduced computational cost and permits larger mesh and time step sizes, a coarser mesh was used for validation. Initially, the mesh size and time step size were varied until the results showed correlation with the data of the two papers. The accuracy of the results also depends on the time step size; therefore, the time step was varied

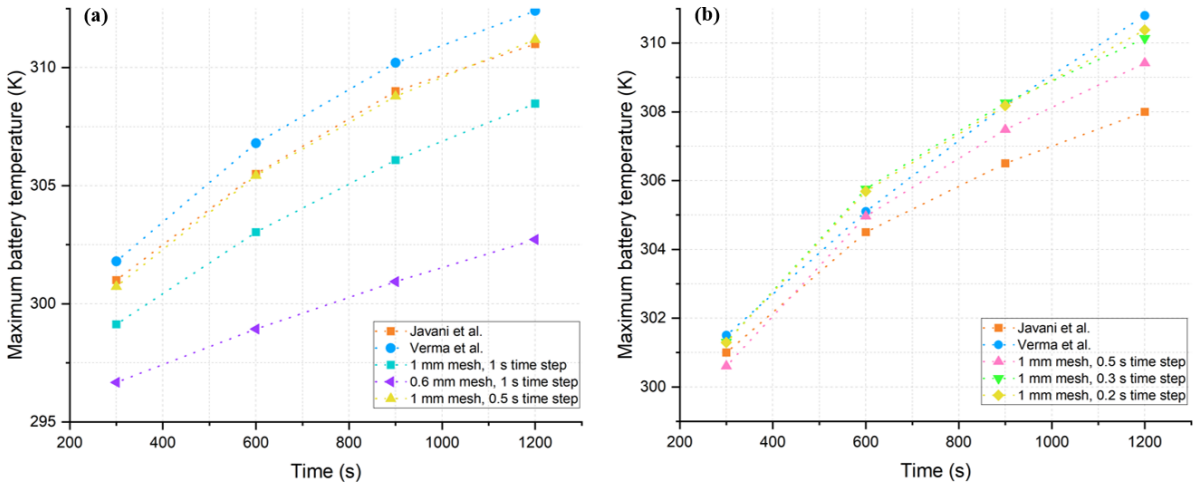

Figure 30. Validation of the battery model a) without and b) with PCM cooling

until the results converged. The maximum temperature of the cell was compared for each case.

To model the cell without PCM cooling, a 1 mm mesh with a 0.5 s time step size was sufficient, as it coincides with results from Javani et al. (2014). However, for the battery model with PCM cooling, the model with 1 mm mesh size and 0.3 s time step was chosen as it gives converged values from the time step convergence study, and the values are close to both results

by Javani et al. (2014) and Verma et al. (2019) with Root Mean Square Error (RMSE) values of 1.53 and 0.48, respectively, hence, the model can be used to obtain reliable results for the EHC model in comparison with the EP model. However, since the EP model requires smaller mesh sizes to generate reliable results, the same mesh element size of 0.6 mm was used for all models for an independent comparison of results.

RESULTS

Error! Reference source not found. presents the temperature distribution of the battery without PCM cooling and with P CM cooling under FlowZ and FlowY configurations at 1800 s. With PCM cooling, the maximum temperature was reduced from 314.12 K to 309.64 K in the FlowZ configuration and to 310.57 K in the FlowY configuration. The location of the maximum temperature shifted upward, attributed to the PCM layer at the bottom. Between the two PCM configurations, FlowZ demonstrated superior cooling performance.

Although at 2C mode, the maximum duration the battery works is for 1800 s, the cooling performance was further analysed for a higher duration to understand the PCM melting behaviours and the cooling performance associated with it.

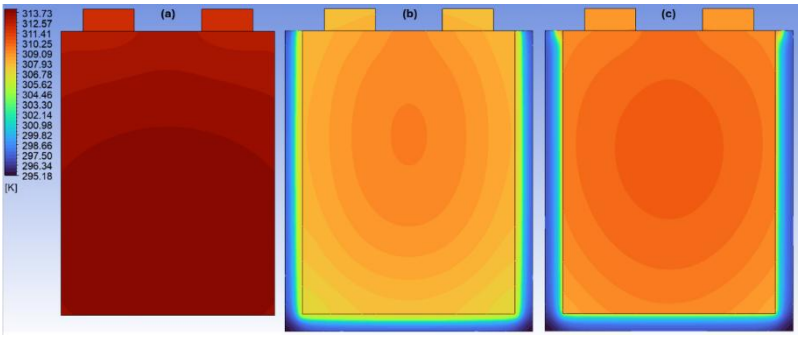

Figure 31. Temperature variation of the cell a) Cellw/oPCM, b) FlowZ config, c) FlowY configurations at 1800

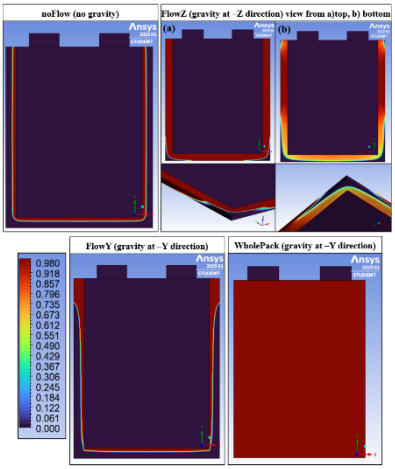

Figure 32. Liquid fraction of PCM for different configurations at 3

Error! Reference source not found. shows the liquid fraction of PCM for different configurations at 3600 s. Figure 33 (a) shows the temperature variation of Point 3 for each PCM configuration and Figure 33 (b) shows the liquid fraction variation

of PCM with time.

Cooling

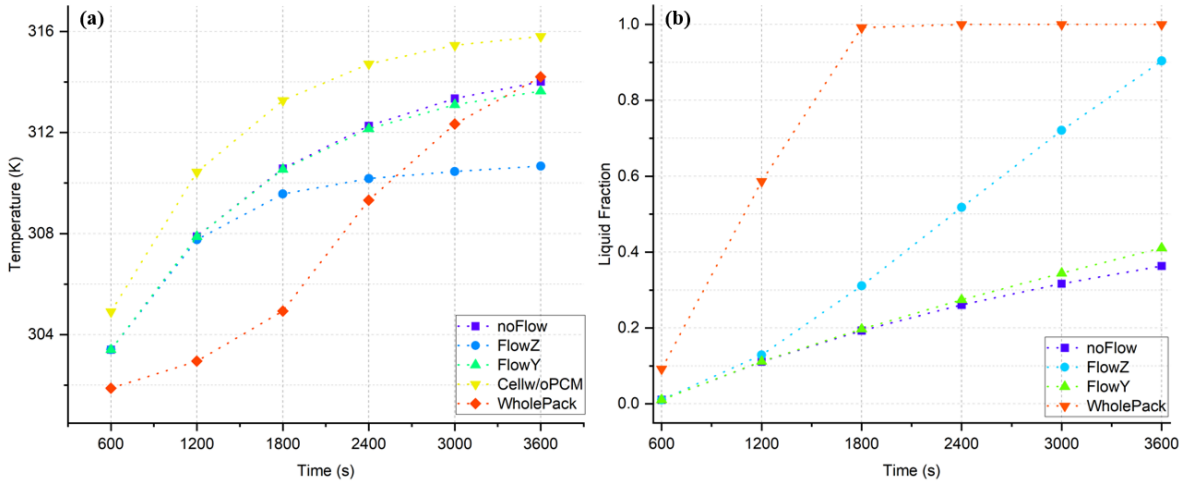

Figure 33. a) Temperature variation at Point 3, b) liquid fraction variation of PCM, for different PCM configurations

Performance Evaluation: EHC Model vs. EP Model

When comparing the temperature-time curves of noFlow, FlowZ, and FlowY in Figure 33(a), the noFlow and FlowZ curves are nearly identical at first, with noticeable differences emerging only at later time steps. The deviation in the FlowZ curve arises from distinct melting behavior driven by convective flow, as illustrated by the liquid fraction graphs in Figure 33(b). Initially, all temperature curves overlap because liquid fractions are low and heat transfer is dominated by conduction, resulting in similar performance across the noFlow, FlowZ, and FlowY models. As melting progresses, however, convective flow begins to significantly influence cooling performance.

Hence, modelling the convective flow is important when evaluating the cooling performance of PCM units. Although the EHC model can be used for small time durations during the initial melting phase to save computational efforts, as the PCM melts, incorporating the effects of convective flow using the EP model is important to accurately predict the thermal performance.

Impact of Cell Orientation on PCM Cooling Efficiency

When structural loading is considered, the vertical orientation is preferred for stacking prismatic cells in a battery pack. However, in terms of cooling performance, the horizontal orientation (FlowZ) outperforms the vertical orientation (FlowY) over the studied duration, as shown in Figure 33(a) and supported by the temperature contours in **Error! Reference source not found.**. The FlowZ configuration achieves higher liquid fractions faster, enabling greater utilization of latent heat for cooling. Convective flow in the horizontal orientation also promotes more effective heat propagation through the thin PCM layer, as illustrated by the melt flow patterns in **Error! Reference source not found.**.

Over the observed duration, the FlowY configuration showed only marginal improvement compared with the conduction-only model. This behavior arises because the melt flow is concentrated near the top of the cell, while the rest of the melting pattern remains similar to the noFlow model. Thus, although convective flow is present in the PCM unit, its impact is limited if it is not well distributed throughout the material. The influence of convection is expected to become more pronounced at higher liquid fractions over longer operating durations.

Comparison of Peripheral vs Fully Encapsulated PCM Configurations

The effect of PCM placement was evaluated, accounting for the orthotropic thermal conductivity of the battery, in two configurations: SidePack and WholePack. As shown in Figure 33 (b), the liquid fraction of the WholePack configuration reached 1 at 1800 s, while all SidePack configurations exhibited slower melting. Consequently, the WholePack initially

demonstrated superior cooling performance. However, once the PCM fully transitioned through the phase change region, the cell temperature increased sharply, emphasizing the importance of designing PCM units to operate effectively within the phase change range. At later stages, the FlowZ configuration outperformed the WholePack, maintaining better cooling performance as melting progressed.

The initial strong performance of the WholePack configuration is attributed to the large heat transfer area available, as the PCM fully encapsulates the battery with a thin layer. In contrast, with the SidePack designs, although the peripheral thermal conductivity of the cell is higher, the inherently low thermal conductivity of the PCM delays heat propagation until sufficient melting occurs to initiate convective flow and enhance thermal transfer.

Hence, the PCM unit should be designed according to the specific requirements of the application, such as operating duration and acceptable temperature range. For applications requiring long-term temperature regulation where minor increments are permissible, the SidePack configuration is more suitable. Conversely, applications demanding strict thermal control over shorter periods would benefit from designs similar to the WholePack. Therefore, a careful evaluation of design requirements is essential for developing an optimized PCM cooling unit. Furthermore, the initial low thermal performance of the SidePack configurations, caused by the low inherent thermal conductivity of the PCM, can be improved by incorporating nanoparticles to enhance conductivity. However, a critical evaluation is required, as the addition of nanoparticles also increases the viscosity of the nanocomposite PCM (NCPCM), thereby reducing thermal convection. Thus, the nanoparticle concentration should be carefully optimized by considering the combined effects of conduction and convection.

Comparison of centerline temperature evolution for all PCM configurations

Figure 34 shows the temperature variation of the cell along the centreline at the five points (Points 1–5) for the four PCM configurations over time. The WholePack configuration exhibited the best cooling performance initially, up to 2400 s, due to the rapid phase change of the PCM enabled by effective thermal propagation and the large heat transfer area. However, its performance declined once the PCM entered the sensible heat storage region.

Among the SidePack configurations, the FlowZ orientation demonstrated the highest cooling efficiency throughout the observed duration. Between 1800 s and 3600 s, FlowZ controlled the temperature rise effectively, showing only a slight increase over time. These results indicate that the horizontal orientation enhances convective flow, improving the ability of PCM to absorb and propagate thermal energy. In the FlowZ configuration, the cooling performance is higher towards the bottom of the cell, caused by the cooling effects of the PCM layer at the bottom.

Initially, at 600 s, all three SidePack configurations exhibited similar behavior, as heat transfer was dominated by conduction, which is consistent across the models. The noFlow and FlowY configurations showed nearly identical performance in the early stages, indicating that the simplified EHC model can be applied to the vertical orientation for a limited duration. However, as the PCM melted, convective flow effects became more pronounced in the FlowY configuration which could no longer be neglected. At higher time steps, the FlowY model demonstrated lower temperatures near the bottom of the cell compared to the noFlow model. This resulted from upward heat transport by the melted PCM, which left the lower region at relatively lower temperatures and thereby improved cooling performance.

Hence, these results provide insight into the impact of convective flow on the cooling performance of PCMs and highlight the importance of modeling it to accurately capture melting patterns and cooling behavior.

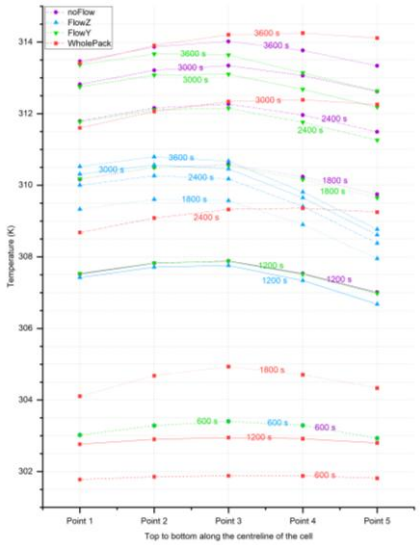

Figure 34. Temperature variation of the cell along the centreline at 600s, 1200 s, 1800 s, 2400 s, 3000 s, 3600 s

CONCLUSION

The cooling performance of different PCM configurations for the thermal regulation of prismatic battery cells was analyzed. Two modelling approaches were considered: the EHC method, which accounts only for thermal conduction in the propagation, and the EP method, which incorporates both conduction and convective flow. The cooling performance results from the two models were compared, and it was found that the simplified EHC method can be used for a limited period of about 1200 s, during which conduction is the dominant heat transfer mechanism. However, as the PCM melts, more complex models that account for convective flow, such as the EP model, are required to capture the melt dynamics and the resulting cooling performance.

Furthermore, two battery orientations, vertical (FlowY) and horizontal (FlowZ), were compared to assess the effect of convective flow on the cooling performance of the PCM unit. The FlowZ configuration exhibited superior cooling, achieving higher liquid fractions over time and resulting in a 3.9 K temperature drop at Point 5, located at the bottom of the cell, after 3600 s. Hence, the horizontal orientation enhances convective flow, enabling more effective heat propagation throughout the PCM unit. However, since the vertical orientation is preferred for prismatic cells due to cell stacking in battery packs, additional techniques are needed to enhance thermal propagation and melt rates in the FlowY configuration. Approaches such as incorporating fins or using graphite/metal foams could be explored to improve heat transfer within the PCM unit.

Finally, two PCM configurations were evaluated using the same PCM volume: a peripheral layer (SidePack) and full encapsulation of the cell (WholePack), to assess the effect of increasing the heat transfer area given the orthotropic thermal conductivity of the cell. The WholePack configuration demonstrated superior cooling performance, achieving a temperature reduction of up to 6.1 K compared with the FlowY orientation, and a maximum cell temperature reduction of 8.3 K relative to the air-cooled battery after 1800 s of operation. These results indicate that the WholePack is more effective than the SidePack in regulating cell temperatures. However, the cooling performance of the WholePack configuration substantially decreased once the PCM fully melted and entered the sensible heat storage region, leading to a gradual temperature rise after 1800 s. In contrast, the SidePack configuration, particularly in the FlowZ orientation, showed lower initial cooling, but delivered better performance with the melting of PCM, with cell temperatures dropping below those of the WholePack

configuration. Hence, the design of the PCM unit should account for the required duration of operation. The WholePack configuration is more suitable for short-term cooling, while the SidePack configuration is preferable for longer durations, as its thicker PCM layer slows heat propagation and sustains latent heat cooling.

Therefore, this study highlights the influence of different PCM cooling unit designs on cooling performance and emphasizes the need to align the design configuration with application requirements. Future work requires enhancing PCM cooling for vertically oriented cells, which are typically preferred in battery packs. Approaches to improve convective flow distribution within the PCM unit, such as optimized fin patterns or the use of metallic/graphite foams should be explored through further computational analysis.

REFERENCES

[1] G. Zaki, E., & S. Dhmees, A. (Eds. . (2022). Paraffin - Thermal Energy Storage Applications (E. G. Zaki & A. S. Dhmees (eds.)). IntechOpen. https://doi.org/10.5772/intechopen.90983

[2] Jaguemont, J., Omar, N., Van den Bossche, P., & Mierlo, J. (2018). Phase-change materials (PCM) for automotive applications: A review. Applied Thermal Engineering, 132, 308–320. https://doi.org/10.1016/j.applthermaleng.2017.12.097

[3] Jankowski, N. R., & McCluskey, F. P. (2014). A review of phase change materials for vehicle component thermal buffering. Applied Energy, 113, 1525–1561. https://doi.org/10.1016/j.apenergy.2013.08.026

[4] Javani, N., Dincer, I., Naterer, G. F., & Yilbas, B. S. (2014). Heat transfer and thermal management with PCMs in a Li-ion battery cell for electric vehicles. International Journal of Heat and Mass Transfer, 72, 690–703. https://doi.org/10.1016/j.ijheatmasstransfer.2013.12.076

[5] Li, W., Yin Yuen, A. C., Li, W., Li, W., Lin, P., Li, A., De Cachinho Cordeiro, I. M., Chen, Q., & Yuan Chen, T. B. (2025). Optimisation of PCM passive cooling efficiency on lithium-ion batteries based on coupled CFD and ANN techniques. Applied Thermal Engineering, 259(November 2024). https://doi.org/10.1016/j.applthermaleng.2024.124874

[6] Pan, C., Charles, J., Vermaak, N., Romero, C., Neti, S., Zheng, Y., Chen, C. H., & Bonner, R. (2018). Experimental, numerical and analytic study of unconstrained melting in a vertical cylinder with a focus on mushy region effects. International Journal of Heat and Mass Transfer, 124, 1015–1024. https://doi.org/10.1016/j.ijheatmasstransfer.2018.04.009

[7] Shirazi, A. H. N., Mohebbi, F., Azadi Kakavand, M. R., He, B., & Rabczuk, T. (2016). Paraffin Nanocomposites for Heat Management of Lithium-Ion Batteries: A Computational Investigation. Journal of Nanomaterials, 2016. https://doi.org/10.1155/2016/2131946

[8] Subramanian, M., Hoang, A. T., B, K., Nižetić, S., Solomon, J. M., Balasubramanian, D., C, S., G, T., Metghalchi, H., & Nguyen, X. P. (2021). A technical review on composite phase change material based secondary assisted battery thermal management system for electric vehicles. Journal of Cleaner Production, 322(September). https://doi.org/10.1016/j.jclepro.2021.129079

[9] Verma, A., Shashidhara, S., & Rakshit, D. (2019). A comparative study on battery thermal management using phase change material (PCM). Thermal Science and Engineering Progress, 11(March), 74–83. https://doi.org/10.1016/j.tsep.2019.03.003

[10] Warner, J. (2014). Lithium-Ion Battery Packs for EVs. In Lithium-Ion Batteries: Advances and Applications. Elsevier. https://doi.org/10.1016/B978-0-444-59513-3.00007-8